sciendo

POLISH MARITIME RESEARCH 2 (110) 2021 Vol. 28; pp. 85-95
10.2478/pomr-2021-0025

INVESTIGATIONS OF THE EMISSION CHARACTERISTICS OF A DUAL-FUEL GAS TURBINE COMBUSTION CHAMBER OPERATING SIMULTANEOUSLY ON LIQUID AND GASEOUS FUELS

Serhiy Serbin*
Badri Diasamidze
Viktor Gorbov
Admiral Makarov National University of Shipbuilding, Ukraine
Jerzy Kowalski
Gdańsk University of Technology, Poland

* Corresponding author: *serbin1958@gmail.com (S. Serbin)*

ABSTRACT

This study is dedicated to investigations of the working process in a dual-fuel low-emission combustion chamber for a floating vessel's gas turbine. As the object of the research, a low-emission gas turbine combustion chamber with partial premixing of fuel and air inside the outer and inner radial-axial swirls was chosen. The method of the research is based on the numerical solution of the system of differential equations which represent the physical process of mass and energy conservation and transformations and species transport for a multi-component chemically reactive turbulent system, considering nitrogen oxides formation and a discrete ordinates model of radiation. The chemistry kinetics is presented by the 6-step mechanism of combustion. Seven fuel supply operating modes, varying from 100% gaseous fuel to 100% liquid fuel, have been analysed. This analysis has revealed the possibility of the application of computational fluid dynamics for problems of dual-fuel combustion chambers for the design of a floating vessel's gas turbine. Moreover, the study has shown the possibility of working in different transitional gaseous and liquid fuel supply modes, as they satisfy modern ecological requirements. The dependencies of the averaged temperature, NO, and CO concentrations along the length of the low-emission gas turbine combustion chamber for different cases of fuel supply are presented. Depending on the different operating modes, the calculated emission of nitrogen oxides NO and carbon monoxide CO at the outlet cross-section of a flame tube are different, but, they lie in the ranges of 31–50 and 23–24 mg/nm^3 on the peak of 100% liquid fuel supply mode. At operating modes where a gaseous fuel supply prevails, nitrogen oxide NO and carbon monoxide CO emissions lie in the ranges of 1.2–4.0 and 0.04–18 mg/nm^3 respectively.

Keywords: gas turbine engine,dual-fuel combustion,combustion chamber,liquid and gaseous fuels

INTRODUCTION

The problem of the design and exploitation of marine power plants of Floating Production, Storage, and Offloading (FPSO) vessels is of interest to the Offshore Gas and Oil industry. A forecast from 2020 to 2024 expects 60 new FPSO vessels projects to go forward, with an expectation that 29 of them will have new-built hulls [1]. Gas turbines are frequently used as FPSO marine power plants, so there is a strong need to create both efficient and ecologically-friendly gas turbines. Despite the existing research on FPSO power plant enhancement [2-8], the current data investigating the burning of dual-fuel in the modern gas turbine combustion chamber and its operating modes applied to FPSO power plants is insufficient. One of the challenging tasks of developing dual-fuel combustion chambers is to provide the required nitrogen oxides concentrations [9] while sustaining low emissions of carbon monoxide and unburned hydrocarbons when operating on various transitional modes of gaseous and liquid fuel supply. Experimental work to investigate the dual-fuel combustion of diesel fuel and methane [10] in internal combustion engines (ICE) has revealed that burning dual-fuel provides lower emission of nitrogen oxide compared to the

diesel fuel operation mode due to the lower flame temperature and lower heat capacity of methane.

This work uses computational fluid dynamics (CFD) methods and is dedicated to the investigation of transitional gaseous and liquid fuel supply modes combining advanced methods of mathematical modelling and the idea of the preliminary simultaneous mixing of liquid and gaseous fuels and air in the radial-axial swirls of a flame tube. Revealing the behaviour of transitional gaseous and liquid fuel supply modes is important for the exploitation of gas turbine engines as they could cause flame instability and flame blowout.

MATHEMATICAL MODELLING

The mathematical modelling of combustion processes in a dual-fuel low-emission combustion chamber for an FPSO includes modelling of the physical and chemical processes. This is based on the solution of the differential equations of mass, impulse, and energy conservation for the multi-component, turbulent, chemically reacting system. The main equations of the gaseous phase model are continuity, the equation of momentum conservation, the energy conservation equation, and the equation for the conservation of chemical components. A detailed description of the equations and methods of solving them in the case of gaseous fuel is given in [7, 11-16]. The transfer equations for the kinetic energy of turbulence k and the dissipation rate of turbulent energy ε for the Renormalization Group (RNG) turbulence model [17] have been chosen. In this article equations that are applied directly to dual-fuel combustion and the interaction of gaseous and liquid phases are noted:

– the continuity equation:

$$\frac{\partial \rho}{\partial t} + \frac{\partial}{\partial x_i}(\rho u_i) = \dot{\rho}^s \tag{1}$$

– the equation of momentum conservation:

$$\frac{\partial}{\partial t}(\rho u_j) + \frac{\partial}{\partial x_i}(\rho u_i u_j) = \frac{\partial}{\partial x_i}\left[\mu\left(\frac{\partial u_i}{\partial x_j} + \frac{\partial u_j}{\partial x_i}\right)\right] - \frac{\partial p}{\partial x_j} + \rho g_i + \dot{F}^s + \frac{\partial}{\partial x_i}(\rho \overline{u_i' u_j'}) \tag{2}$$

– the energy conservation equation:

$$\frac{\partial}{\partial t}(\rho h_0) + \frac{\partial}{\partial x_i}(\rho u_i h_0) = \frac{\partial}{\partial x_i}\frac{k_m + k_t}{c_p}\left[\frac{\partial (h_0 - u^2/2)}{\partial x_i} - \sum_j h_j \frac{\partial X_j}{\partial x_i}\right] - \tag{3}$$
$$- \frac{\partial}{\partial x_i}\sum_j h_j J_{ji} + \frac{\partial p}{\partial t} - \frac{\partial}{\partial x_i}(\tau_{ik} u_k) + S_h + \dot{Q}^s,$$

– the equation for the conservation of chemical components:

$$\frac{\partial}{\partial t}(\rho Y_i) + \frac{\partial}{\partial x_i}(\rho u_i Y_i) = \frac{\partial}{\partial x_i} J_i + R_i + \dot{\rho}^s \delta_i \tag{4}$$

In Eqs. (1)–(4), t is the time; x_i and x_j are the coordinates; ρ, u, μ, p, and g are the density, velocity, viscosity, pressure, and gravity acceleration; $\dot{\rho}^s$, $\dot{F}^s$, $\dot{W}^s$, and $\dot{Q}^s$ are the sources for the interaction of the gas and liquid phases; G_k is the source describing the generation of turbulent energy; C_1, C_2, and C_s are the empirical constants; h_0 is the stagnation enthalpy; h_j is the component's enthalpy; k_m and k_t are the coefficients of molecular and effective thermal conductivity; c_p is the specific heat of the mixture at constant pressure; τ_{ik} is the shear stress tensor; J_{ji} is the component j flow in the i direction; S_h is the source term from the chemical reaction; Y_i is the mass fraction of component i; R_i is the rate of the component's formation or destruction; J_i is the diffusion component's flow; and δ_i is the Dirac delta function.

The net source of chemical species i due to the reaction is computed as the sum of the Arrhenius reaction sources over the N_r reactions in which the species participate:

$$R_i = M_{w,i} \sum_{r=1}^{N_R} R_{i,r} \tag{5}$$

where $M_{w,i}$ is the molecular weight of species i and $R_{i,r}$ is the Arrhenius molar rate of creation/destruction of species i in reaction r.

Consider the r-th reaction written in the general form:

$$\sum_{i=1}^{N} v_{i,r}' M_i \underset{k_{f,r}}{\overset{k_{b,r}}{\Leftrightarrow}} \sum_{i=1}^{N} v_{i,r}'' M_i \tag{6}$$

where N is the number of chemical species in the system; $v_{i,r}'$ is the stoichiometric coefficient for reactant i in reaction r; $v_{i,r}''$ is the stoichiometric coefficient for the product i in reaction r; M_i is the symbol denoting species i; $k_{f,r}$ is the forward rate constant for reaction r; and $k_{b,r}$ is the backward rate constant for reaction r.

For a non-reversible reaction, the molar rate of creation/destruction of species i in reaction r is given by

$$R_{i,r} = \Gamma\left(v_{i,r}'' - v_{i,r}'\right) \cdot \left(k_{f,r} \prod_{j=1}^{N} \left[C_{j,r}\right]^{(\eta_{j,r}' + \eta_{j,r}')}\right) \tag{7}$$

where $C_{j,r}$ is the molar concentration of species j in reaction r; $\eta_{j,r}'$ is the rate exponent for reactant species j in reaction r; $\eta_{j,r}''$ is the rate exponent for product species j in reaction r; and Γ presents the net effect of third bodies on the reaction rate:

$$\Gamma = \sum_j^{N_r} \gamma_{j,r} C_j \tag{8}$$

where $\gamma_{j,r}$ is the third-body efficiency of the j-th species in the reaction r.

Modelling of nitrogen oxides emissions was carried out using transfer equations which include convection, diffusion, formation, and decomposition of NO and related compounds. The influence of the reaction volume's residence time on the mechanism of nitrogen oxide formation is considered in the convection terms of the defining equations written in the Euler reference system. For thermal and prompt nitrogen oxides, it is necessary to solve the NO transfer equation [11, 16]:

$$\frac{\partial}{\partial t}(\rho Y_{\mathrm{NO}}) + \nabla \cdot (\rho \vec{v} Y_{\mathrm{NO}}) = \nabla \cdot (\rho D \nabla Y_{\mathrm{NO}}) + S_{\mathrm{NO}} \tag{9}$$

where Y_{NO} is the NO mass fraction; D is the diffusion coefficient; $\vec{v}$ is the velocity vector; and S_{NO} is the source term depending on the NO formation mechanism.

The eddy dissipation combustion (EDC) model [18] and its detailed chemical mechanisms in turbulent flows are included in this research. It assumes that the reaction occurs in small turbulent structures, called fine scales. The length fraction of the fine scales is modelled as

$$\xi^* = C_\xi(\nu\varepsilon/k^2)^{0.75} \quad (10)$$

where $C_\xi = 2.1377$ is the volume fraction constant and ν is the kinematic viscosity.

Species are assumed to react in the fine structures over a time scale

$$\tau^* = C_\tau(\nu/\varepsilon)^{0.5} \quad (11)$$

where $C_\tau = 0.4082$ is the time-scale constant.

The length fraction of the fine scales is modelled as reactions proceed over the time scale, governed by the Arrhenius rates, and are integrated numerically using the ISAT algorithm [19]. The validity of the EDC approach for modelling physicochemical processes is demonstrated for two-phase turbulent swirling liquid spray burning in a complex gas turbine combustion chamber [20] and for a model gas turbine combustor [21].

To simulate the formation of carbon monoxide and molecular hydrogen inside a dual-fuel gas turbine combustion chamber, it is proposed to use the 6-step kinetic mechanism for simultaneous combustion of liquid and gaseous fuels:

$$2\ C_{16}H_{29} + 16\ O_2 \rightarrow 32\ CO + 29\ H_2 \quad (12)$$

$$2\ H_2 + O_2 \rightarrow 2\ H_2O \quad (13)$$

$$2\ CO + O_2 \rightarrow 2\ CO_2 \quad (14)$$

$$2\ H_2O \rightarrow 2\ H_2 + O_2 \quad (15)$$

$$2\ CO_2 \rightarrow 2\ CO + O_2 \quad (16)$$

$$2\ CH_4 + O_2 \rightarrow 2\ CO + 4\ H_2O \quad (17)$$

The reaction rate constants of the proposed kinetic mechanism are presented in Table 1.

Validation of similar global chemical mechanisms for the conditions of a gas turbine combustion chamber was carried out in several investigations [11, 22-24]. These works have shown the applicability of kinetic mechanisms to study the combustion of liquid and gaseous fuels in gas turbine combustion chambers in a wide range of variations of the governing parameters.

For calculations of liquid fuel combustion in a low-emission combustion chamber, the Discrete Phase Model (DPM), which calculates the trajectories of motion for individual particles, was selected [18, 25, 26]. The model predicts the particle trajectories of the discrete phase by integrating their motion equations written in the Lagrange form [18, 25-27].

In this study, the discrete ordinates (DO) radiation model is chosen. The DO model (20) considers the radiative transfer equation (RTE) (19) as a field equation and solves it for nine discrete solid angles, each associated with a vector direction $\vec{s}$ fixed in the global Cartesian system (x, y, z).

The radiative transfer equation for an absorbing, emitting, and scattering medium at the position $\vec{r}$ in the direction $\vec{s}$ as field equation [28]:

$$\frac{\partial I(\vec{r}\vec{s})}{\partial s} + (a+\sigma_s)(I\vec{r}\vec{s}) = an^2\frac{\sigma T^4}{4\Pi} + \frac{\sigma_s}{4\Pi}\int_0^{4\Pi}\left(I(\vec{r}\,\vec{s'})\Phi(\vec{s}\cdot\vec{s'})\right)d\Omega' \quad (18)$$

where $\vec{r}$ is the position vector; $\vec{s}$ is the direction vector; $s'$is the scattering direction vector; s is the path length; a is the absorption coefficient; n is the refractive index; σ_s is the scattering coefficient; σ is the Stefan–Boltzmann constant; I is the radiation intensity, which depends on the position $\vec{r}$ and direction $\vec{s}$; T is the local temperature; Φ is the scattering phase function; Ω is the solid angle.The discrete ordinates model equation

$$\nabla\cdot(I\vec{r}\vec{s})\vec{s} + (a+\sigma_s)(I\vec{r}\vec{s}) = an^2\frac{\sigma T^4}{4\Pi} + \frac{\sigma_s}{4\Pi}\int_0^{4\Pi}\left(I(\vec{r}\,\vec{s'})\Phi(\vec{s}\cdot\vec{s'})\right)d\Omega' \quad (19)$$

where $(I\vec{r}\,\vec{s})$ is the total intensity; Φ is the scattering phase function.

For simplicity, it is assumed that the temperature of the droplet does not change when boiling. The energy required for evaporation is taken into consideration as a source term in the equation for the energy conservation of the gas phase. Liquid evaporation is also a source of chemical component for the gas phase. A detailed description of the research object and verification of the mathematical model are given in [7].

Tab. 1. Reaction rate constants for a six-stage oxidation mechanism of diesel fuel and methane

Reaction	A	E, J/mol	β	The order of the reaction			
$2\ C_{16}H_{29} + 16\ O_2 \rightarrow 32\ CO + 29\ H_2$	1.1206e+19	1.2238e+08	2.541	$C_{16}H_{29}$	2.066	O2	1.953
$2\ H_2 + O_2 \rightarrow 2\ H_2O$	9.1048e+14	2.7007e+08	0.467	H_2	0.57	O2	1.178
$2\ CO + O_2 \rightarrow 2\ CO_2$	6.2327e+14	8.4199e+07	-0.309	CO	1.736	O2	1.804
2 H2O -> 2 H_2 + O2	6.5724e+19	3.6931e+08	-0.068	H_2O	2.868		
$2\ CO_2 \rightarrow 2\ CO + O_2$	6.7299e+11	3.5065e+08	-0.255	CO_2	1.871		
$2\ CH_4 + O_2 \rightarrow 2CO + 4H_2O$	9.9126e+14	2.9825e+08	2.618	CH_4	1.109	O2	1.572

We should note that some submodels of the general mathematical model were used by the authors to analyse the working processes of various fuel combustion devices [29-32].

INVESTIGATION OF CHARACTERISTICS OF WORKING PROCESSES IN A DUAL-FUEL COMBUSTION CHAMBER

A low-emission combustion chamber with partial preliminary mixing of fuel and air for a 25 MW UGT25000 gas turbine engine produced by Zorya-Mashproekt was chosen as the object of investigation [16, 33]. The combustion chamber has a cannular counterflow structure (Fig. 1), which implements the principle of dry combustion of a partially mixed lean mixture. The combustion chamber has 16 flame tubes evenly spaced around the engine axis. The total airflow through a combustion chamber at the nominal operating mode is 69.68 kg/s. Compressed air goes to the flame tube through the air inlet and is mixed with a mixture of gaseous and liquid fuel. Gaseous fuel is supplied through a series of holes made in the blades of the radial-axial swirlers of the first and second channels. Liquid fuel is injected using 30 injectors evenly spaced in the sections of the inner and outer swirlers. The design of the flame tube is presented in Fig. 2.

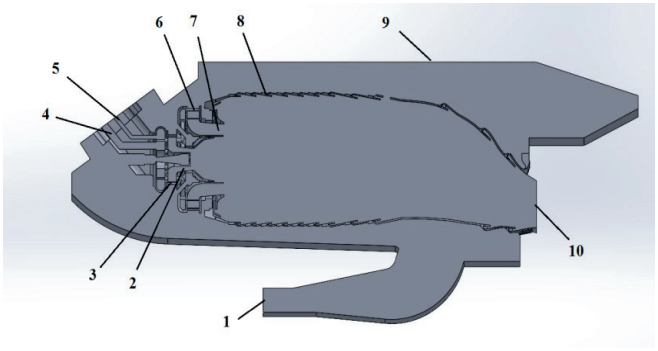

Fig. 1. Longitudinal section of the combustion chamber: 1 – compressed air inlet; 2, 7 – sectors for supplying liquid fuel into the swirlers; 3, 6 – inner and outer radial-axial swirlers; 4, 5 – first and second gaseous fuel channels; 8 – flame tube; 9 – casing; 10 – outlet

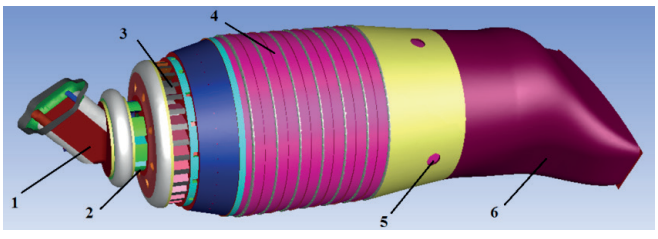

Fig. 2. Flame tube design features: 1 – burner; 2 – inner swirler; 3 – outer swirler; 4 – cooled shells; 5 – dilution air holes; 6 – flame tube diffuser

Since all flame tubes have an identical design, three-dimensional CFD calculations in order to reduce computing resources were carried out for a 1/16 part of a combustion chamber. The initial conditions for a 1/16 part of a low-emission combustion chamber of a 25 MW gas turbine engine are set as follows: the air temperature at the compressed air inlet of 770 K, the pressure of 2.0523 MPa, the airflow of 4.355 kg/s. In the calculations in which the mass fraction of liquid fuel exceeds the mass fraction of gaseous fuel, the liquid fuel consumption through the fuel supply pipes was 358.02 kg/h. In the calculations where the mass fraction of gaseous fuel exceeds the mass fraction of liquid, the consumption was taken as equal to 320.46 kg/h. These parameters correspond to the nominal mode of operation of the gas turbine engine. To simplify the calculations, the flame tube walls were taken as adiabatic. Typical root mean square (RMS) residuals to establish the solution convergence are about $1e^{-4}$.

Fig. 3 shows the locations of the injectors for spraying liquid fuel into the combustion chamber. In the simulation of liquid fuel, a hollow-cone fuel injection method is used, which simulates the spraying of injectors installed in radial-axial swirlers. Parameters of diesel fuel spraying that are common to all operating modes where liquid fuel is supplied are as follows: droplet velocity 15 m/s, the temperature of the diesel fuel 313 K, fuel spray angle 5°. The initial diameters of the fuel droplets are taken from 5 to 75 μm, with an average diameter of 35 μm. Such parameters could be provided by air-mechanical spray nozzles, which are widely used to intensify the processes of breaking liquid fuel droplets and mixing them with an oxidant. Note that 95% of the liquid fuel is fed in the axial direction through fifteen injectors located in the outer swirlers, and 5% of the fuel – through fifteen nozzles located in the inner swirlers.

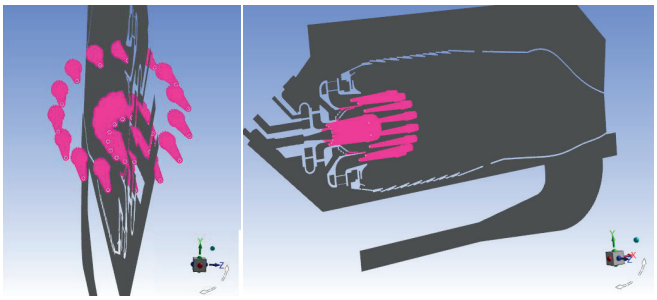

Fig. 3. Injector layout

Modes of simultaneous operation on liquid and gaseous fuels at different ratios of their mass flow through the flame tube were studied. Let us denote by numbers the various modes of fuel supply to the combustion chamber. Mode 1 corresponds to 100% gaseous fuel feeding, mode 2 – 90% gaseous fuel and 10% liquid fuel, mode 3 – 70% gaseous fuel and 30% liquid fuel, mode 4 – 50% gaseous fuel and 50% liquid fuel, mode 5 – 30% gaseous fuel and 70% liquid fuel, mode 6 – 10% gaseous fuel and 90% liquid fuel, and mode 7 – 100% liquid fuel feeding. In all cases, the temperature of the gaseous fuel was taken equal to 288 K.

The gaseous and liquid fuel consumption is presented in Table 2.

Tab. 2. Fuel consumption through the flame tube

Modes of fuel supply	Fuel consumption through the flame tube, kg/s			
	Gaseous fuel		Liquid fuel	
	Outer swirler	Inner swirler	Outer swirler	Inner swirler
1	0.084567	0.004451	0	0
2	0.076110	0.004006	0.000564	0.000029
3	0.059197	0.003116	0.001691	0.000089
4	0.047239	0.002486	0.003149	0.000166
5	0.028343	0.001492	0.004409	0.000232
6	0.009448	0.000497	0.005669	0.000298
7	0	0	0.094477	0.004972

Fig. 4 shows liquid particle traces in the longitudinal section of the flame tube, depending on the modes of fuel supply, taking into consideration the features of mixing the liquid fuel with the mixture of the gaseous fuel and the oxidiser in the channels of the radial-axial swirlers. Due to the nature of the gaseous fuel and its calorific value, modes where the mass fraction of gaseous fuel exceeds 50% are characterised by more intense evaporation of liquid fuel particles.

Tab. 3. Parameters at the outlet combustion chamber section

Mode of fuel supply	1	2	3	4	5	6	7
T_{exit}, K	1564	1555	1532	1610	1608	1578	1565
NO, mg/nm^3	4.59	1.2359	4.8785	19.226	31.332	36.219	49.823
CO, mg/nm^3	0.0438	5.6408	17.813	25.2	23.608	21.083	24.452
δ	0.1407	0.1029	0.1436	0.105	0.1803	0.1267	0.13

The results of three-dimensional modelling are presented in Figs. 5–10.

Figs. 5–7 represent the distribution of the temperature, the mass fractions of carbon monoxide and nitrogen oxide on the axis of the combustion chamber. It can be seen that the temperature in the cross-section of the flame tube for all cases is in the range from 1170 to 1750 K (Fig. 5). Modes of supply in which the amount of gaseous fuel exceeds the amount of liquid fuel are characterised by better mixing of fuel with oxidant and a higher rate of the chemical reaction. Along the length of the flame tube, the concentrations of carbon monoxide decrease monotonically (Fig. 6), which indicates the active combustion of fuel. Note that modes with

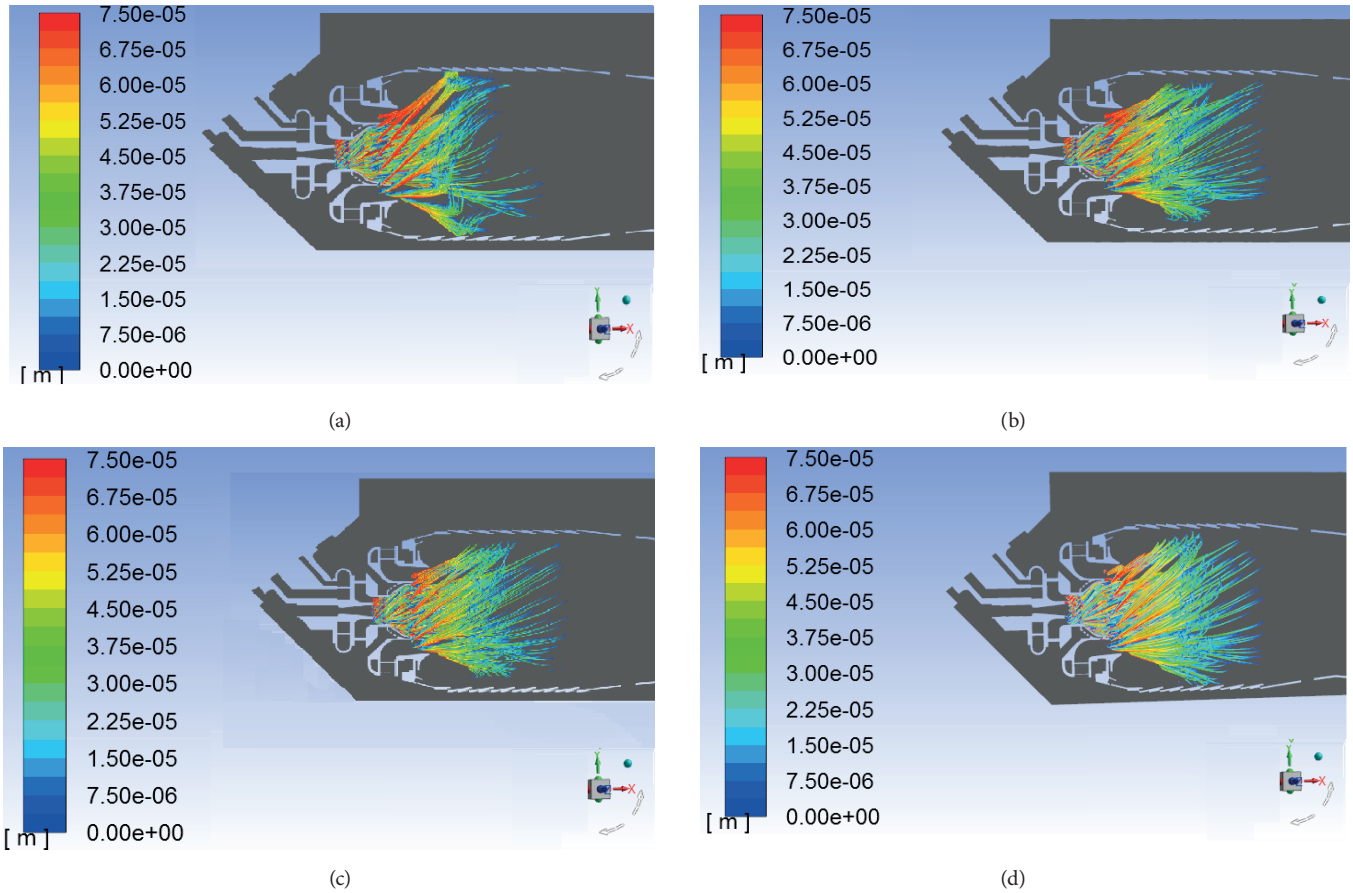

Fig. 4. Particle diameter distribution for different modes of fuel supply: a) 2; (b) 4; (c) 6; (d) 7

The parameters of the combustion products for the outlet section of the flame tube (average temperature of gases T_{exit}, the mass concentrations of nitrogen oxides NO and carbon monoxide CO, the average coefficient of the temperature field non-uniformity d) are presented in Table 3.

a lower proportion of liquid fuel compared to gaseous fuel are characterised by lower concentrations of carbon monoxide.

Fuel supply modes in which the amount of liquid fuel dominates are characterised by higher concentrations of nitrogen oxides in the outlet section of the flame tube due

to the increase in the residence time of reagents in high-temperature zones as a result of delaying the evaporation of liquid fuel and mixing of the evaporated fraction with air. The concentrations of nitrogen oxides NO along the length of the combustion chamber increase (Fig. 6). This is due to the increase in the residence time of the reagents in the primary and secondary zone of the chamber. In the cross-sections of the dilution air supply (the distance from the beginning of the flame tube is 0.32 m) there is a decrease in NO concentrations even on the axis of the chamber as a result of mixing the air and reducing the temperature of the mixture (Fig. 5), and then their further growth is observed. A characteristic trend is that with the increase of liquid fuel content, the concentrations of nitrogen oxides and carbon monoxide in the outlet cross-sections of the flame tube are increasing (Figs. 6, 7).

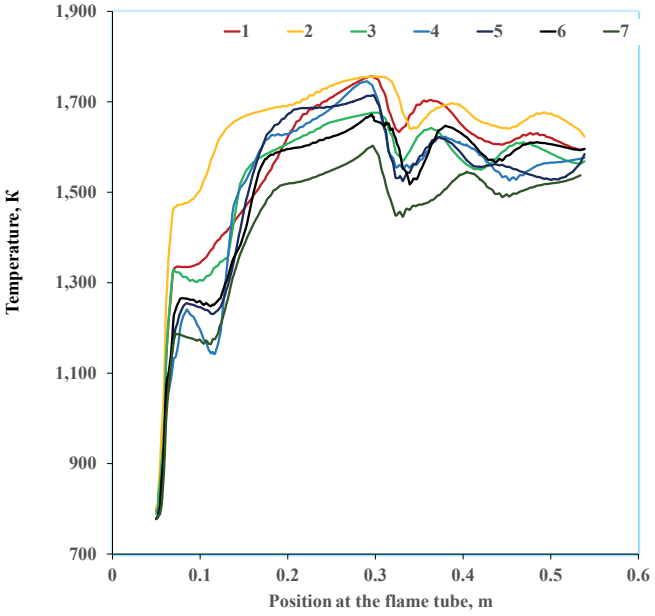

Fig. 5. Distribution of the temperatures (K) along the length of the low-emission combustion chamber for different modes of fuel supply

Figure 8 shows the temperature contours in the longitudinal section of a dual-fuel combustion chamber for four modes of supply of gaseous and liquid fuels. It is seen that the processes of fuel combustion in the cases of the gaseous fuel supply are completed faster, as evidenced by the greater filling of the primary zone with combustion products with high temperatures. As the amount of liquid fuel increases, the flame front is concentrated with the zones corresponding to the trajectories of the fuel droplets, which gradually evaporate and burn in the stream. Moreover, for modes with the vast majority of liquid fuel the maximum combustion products temperature lies in the range of 2100–2280 K, and for modes with a greater amount of gaseous fuel the peak temperatures in the longitudinal cross-section of the combustion chamber are in the range of 1900–2000 K (Fig. 8).

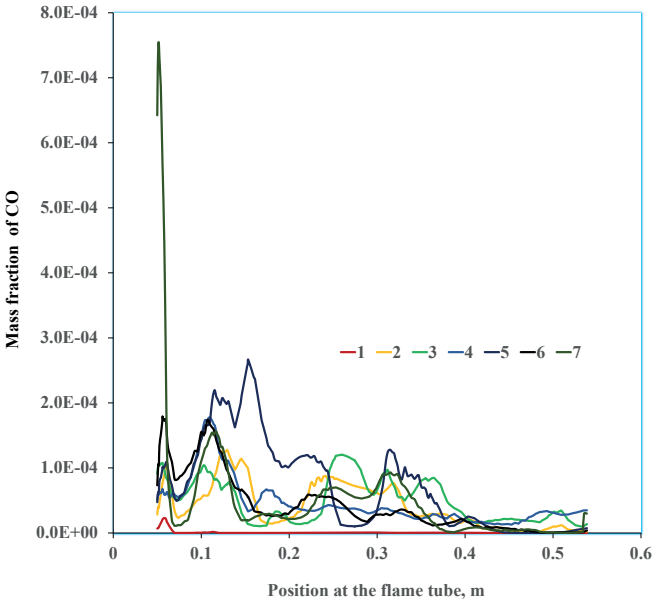

Fig. 6. Distribution of the averaged mass fractions of carbon monoxide along the length of the low-emission combustion chamber for different modes of fuel supply

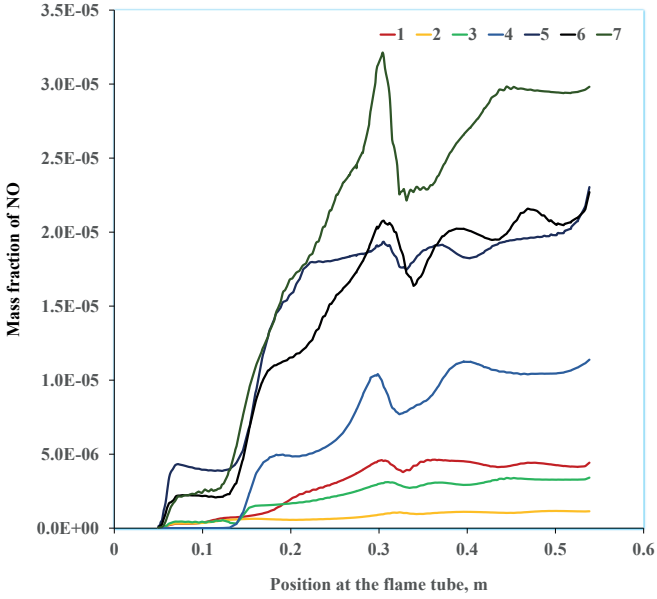

Fig. 7. Distribution of the averaged mass fractions of nitrogen oxide along the length of the low-emission combustion chamber for different modes of fuel supply

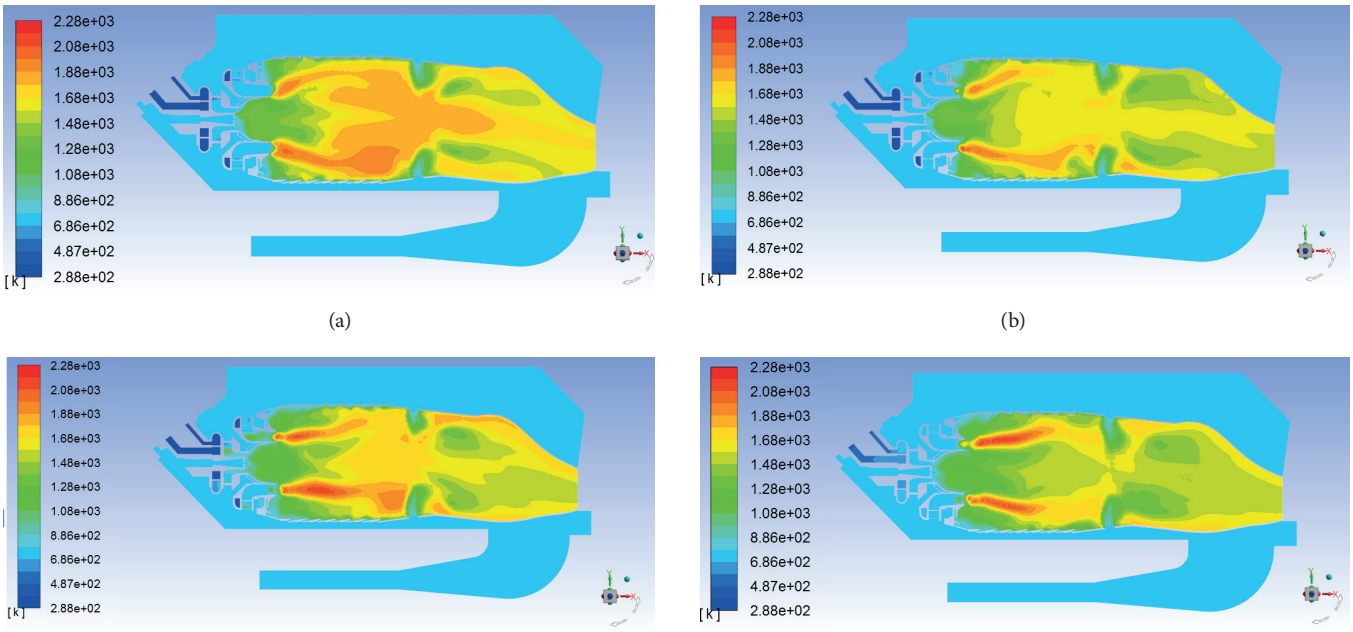

Fig. 8. Distribution of gas temperatures along the flame tube at different fuel supply modes: (a) – 1; (b) – 3; (c) – 5; (d) – 7

Fig. 9 shows the contours of the mass fractions of nitrogen oxides NO in the longitudinal section of the flame tube of the dual-fuel combustion chamber for four modes of supply of gaseous and liquid fuels. In the case of the supply of only gaseous fuel (operating mode 1), the formation of nitrogen oxides is negligible. As the amount of liquid fuel increases, the concentrations of nitrogen oxides increase, and their maximum value is observed in the primary zone of the combustion chamber in the area of the flame front. This confirms that the main mechanism of formation of nitrogen oxides is thermal, which is determined by the maximum temperatures in the flame front.

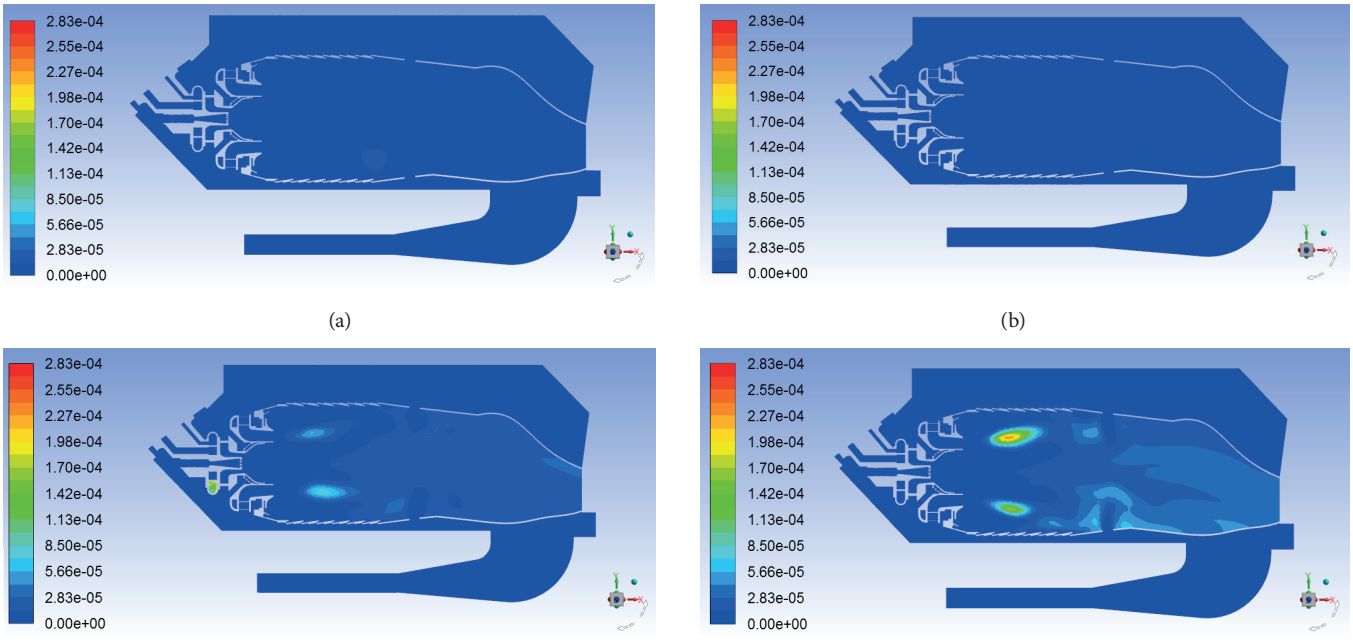

Fig. 9. Distribution of mass fraction of NO along the flame tube at different fuel supply modes: (a) – 1; (b) – 3; (c) – 5; (d) – 7

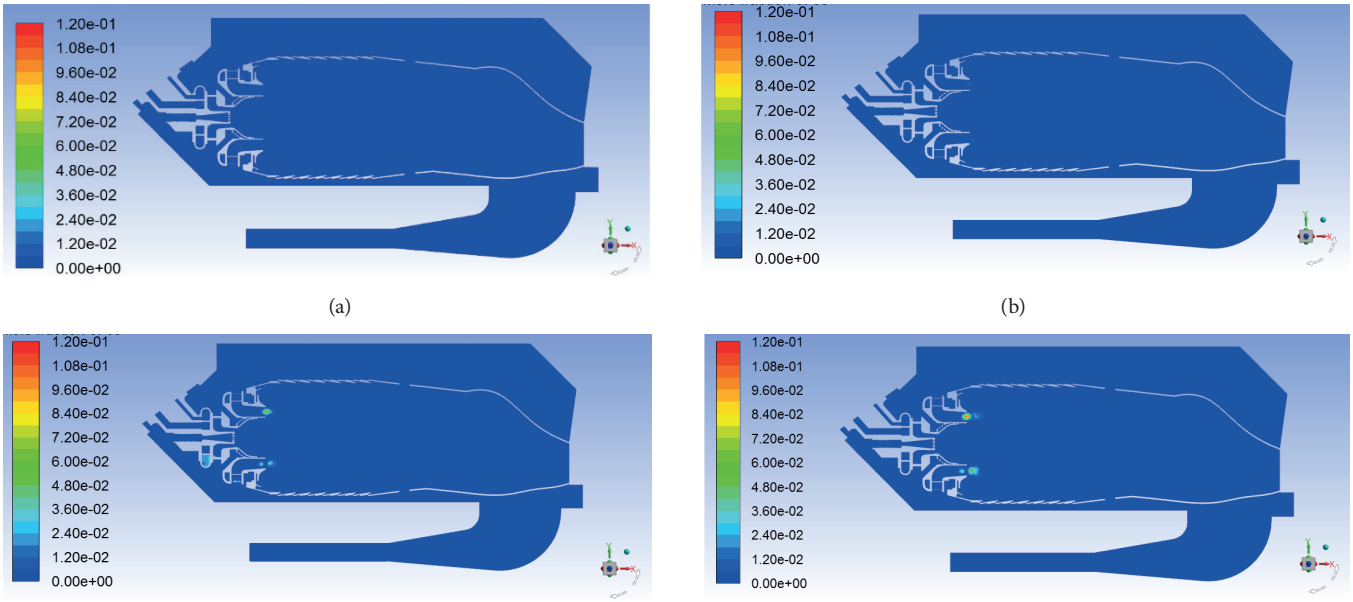

Fig. 10. Distribution of mass fraction of CO along the flame tube at different fuel supply modes: (a) – 1; (b) – 3; (c) – 5; (d) – 7

Fig. 10 shows the contours of the carbon monoxide mass fraction in the longitudinal section of the flame tube for the same modes of supply of gaseous and liquid fuels. It is seen that with the increasing amount of liquid fuel, carbon monoxide CO is mostly formed in local areas located behind the outer swirler. Later, as a result of the active chemical reaction, the CO concentrations decrease sharply.

Fig. 11 shows the calculated dependencies of the NO and CO concentrations (at 15% O_2, dry basis) and the average coefficient of the temperature field non-uniformity δ at the outlet combustion chamber's section on the fuel supply modes.

It should be noted that the coefficient of the average temperature field non-uniformity is determined by the formula

$$\delta = \frac{T_{max} - T_{min}}{T_{av}} \tag{21}$$

where T_{max}, T_{min} and T_{av} are the maximum, minimum, and average gas temperature in the outlet flame tube's section.

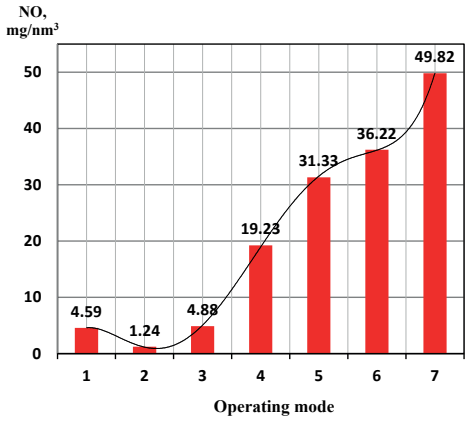

a)

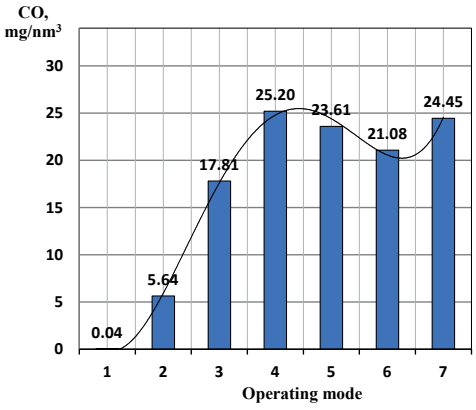

b)

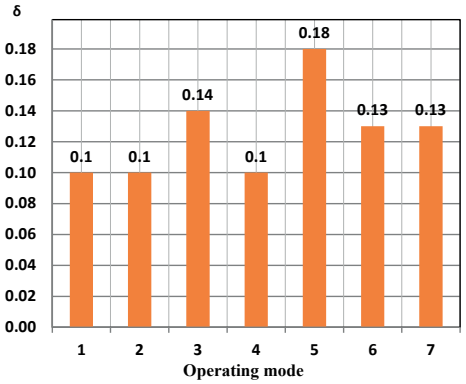

c)

Fig. 11. Combustion chamber's outlet parameters at different fuel supply modes: (a) and (b) – NO and CO concentration at 15% O2, dry basis; (c) – coefficient of the temperature field non-uniformity

The graphic data in the diagrams of Fig. 11 show a significant dependence of the emission of toxic components on the fuel supply mode. The emission of nitrogen oxides increases monotonically with increasing liquid fuel content, while the emission of carbon monoxide in modes with a significant amount of liquid diesel fuel is stabilising. The rate of non-uniformity of the temperature field behind the combustion chamber tends to increase slightly during the transition from gaseous to liquid fuel.

The performance of a dual-fuel combustion chamber can be improved by using various combustion intensifiers, including plasma-chemical devices [34-37]. This is especially important when working on liquid fuel, when there is a need for additional stabilisation of the flame front and an increase in the rate of combustion of evaporating fuel.

CONCLUSIONS

To sum up, the results that have been obtained in this article are as follows:

1. The distributions of temperatures, concentrations of complete combustion products, and toxic components in sections of a dual-fuel combustion chamber for a floating vessel's gas turbine when working on different modes of supply of liquid and gaseous fuels are obtained.
2. To model the process of hydrocarbons burning in a dual-fuel combustion chamber a six-step kinetic mechanism is proposed.
3. The results of mathematical modelling of the workflow processes in a dual-fuel combustion chamber are obtained. The need to use air-mechanical spray nozzles is shown, which can provide a spray spectrum of fuel droplets from 5 to 75 μm with an average diameter of 35 μm or less.
4. Three-dimensional modelling made it possible to identify trends in the formation of toxic components in transient combustion modes from gaseous to liquid fuel. For transient modes with a higher content of gaseous fuel, the estimated emissions of nitrogen oxides NO in the outlet cross-section of the flame tube are 1.2–4.8 mg/nm3, and carbon monoxide 0.04–18 mg/nm3. For transient modes with a higher content of liquid fuel, the estimated emissions of nitrogen oxides NO are 31–50 mg/nm3, and carbon monoxide 23–24 mg/nm3, respectively.
5. The obtained concentrations of the main toxic components of a dual-fuel gas turbine combustion chamber satisfy modern European requirements for emissions of toxic components.
6. High-quality spraying of liquid fuel provides decent overall temperature-field non-uniformity in the outlet section. Still, it could be optimised by using plasma-assisted combustion, which could be a topic for further investigation.

REFERENCES

1. A. Duggal and J. Minnebo, 'The Floating Production, Storage and Offloading system – past, present and future', in *Offshore Technology Conference, Houston, Texas, USA, May 05, 2020*, 2020, doi.org/10.4043/30514-MS.

2. M. M. L. Reis and W. L. R. Gallo, 'Study of waste heat recovery potential and optimization of the power production by an organic Rankine cycle in an FPSO unit', *Energy Convers. Manag.*, vol. 157, pp. 409–422, 2018, doi.org/10.1016/j.enconman.2017.12.015.

3. O. Cherednichenko, S. Serbin, and M. Dzida, 'Application of thermo-chemical technologies for conversion of associated gas in diesel-gas turbine installations for oil and gas floating units', *Pol. Marit. Res.*, vol. 26, no. 3, pp. 181–187, 2019, doi.org/10.2478/pomr-2019-0059.

4. M. Aligoodarz, M. Soleimanitehrani, H. Karrabi, and F. Ehsaniderakhshan, 'Numerical simulation of SGT-600 gas turbine combustor, flow characteristics analysis, and sensitivity measurement with respect to the main fuel holes diameter', *Proc. Inst. Mech. Eng. G J. Aerosp. Eng.*, vol. 230, no. 13, pp. 2379–2391, 2016, doi.org/10.1177/0954410015625663.

5. O. Cherednichenko, S. Serbin, and M. Dzida, 'Investigation of the combustion processes in the gas turbine module of an FPSO operating on associated gas conversion products', *Pol. Marit. Res.*, vol. 26, no. 4, pp. 149–156, 2019, http://doi.org/10.2478/pomr-2019-0077, doi.org/10.2478/pomr-2019-0077.

6. J. A. Vidoza, J. G. Andreasen, F. Haglind, M. M. L. dos Reis, and W. Gallo, 'Design and optimization of power hubs for Brazilian off-shore oil production units', *Energy (Oxf.)*, vol. 176, pp. 656–666, 2019.

7. C. Waldhelm, 'Application of gas turbines on floater vessel for power generation service', in *ASME 1998 International Gas Turbine and Aeroengine Congress and Exhibition*, *Volume 2: Aircraft Engine; Marine; Microturbines and Small Turbomachinery*, 1998.

8. S. Serbin, B. Diasamidze, and M. Dzida, 'Investigations of the working process in a dual-fuel low-emission combustion chamber for an FPSO gas turbine engine', *Pol. Marit. Res.*, vol. 27, no. 3, pp. 89–99, 2020.

9. Directive 2013/39/EU of the European Parliament and of the Council, *Europa.eu*, 2008. [Online]. Available: https://eur-lex.europa.eu/LexUriServ/LexUriServ.do?uri=OJ:L:2013:226:0001:0017:EN:PDF. [Accessed: 05 Mar 2021].

10. S. Di Iorio, A. Magno, E. Mancaruso, and B. M. Vaglieco, 'Analysis of the effects of diesel/methane dual fuel

combustion on nitrogen oxides and particle formation through optical investigation in a real engine', *Fuel Process. Technol.*, vol. 159, pp. 200–210, 2017.

11. S. I. Serbin, 'Modeling and experimental study of operation process in a gas turbine combustor with a plasma-chemical element', *Combust. Sci. Technol.*, vol. 139, no. 1, pp. 137–158, 1998.

12. B. T. Diasamidze, S. V. Vilkul, and S. I. Serbin, 'Theoretical investigations of a dual-fuel low-emission gas turbine combustor', *NTU KhPI Bull. Power Heat Eng. Process. Equip.*, no. 1, pp. 27–33, 2020.

13. C. K. Law, *Combustion Physics*. Cambridge, England: Cambridge University Press, 2010.

14. J. Warnatz, U. Maas, and R. W. Dibble, *Combustion: Physical and chemical fundamentals, modeling and simulation, experiments, pollutant formation*, 3rd ed. Berlin, Germany: Springer, 2013.

15. B. E. Launder and D. B. Spalding, *Lectures in Mathematical Models of Turbulence*. London: Academic Press.

16. S. I. Serbin, I. B. Matveev, and G. B. Mostipanenko, 'Investigations of the working process in a 'lean-burn' gas turbine combustor with plasma assistance', *IEEE Trans. Plasma Sci. IEEE Nucl. Plasma Sci. Soc.*, vol. 39, no. 12, pp. 3331–3335, 2011.

17. D. Choudhury, *Introduction to the Renormalization Group Method and Turbulence Modeling.* Fluent Incorporated, 1973.

18. B. Magnussen, 'On the structure of turbulence and a generalized eddy dissipation concept for chemical reaction in turbulent flow', in *19th Aerospace Sciences Meeting*, *St Louis, MO, USA*,1981.

19. S. B. Pope, 'Computationally efficient implementation of combustion chemistry using in situ adaptive tabulation', *Combust. Theory Model.*, vol. 1, no. 1, pp. 41–63, 1997.

20. F. Wang, Y. Huang, and T. Deng, 'Gas turbine combustor simulation with various turbulent combustion models', in *ASME Turbo Expo 2009: Power for Land, Sea, and Air, June 8–12, 2009, Orlando, Florida, USA*, *Volume 2: Combustion, Fuels and Emissions*, 2009.

21. A. C. Benim, S. Iqbal, W. Meier, F. Joos, and A. Wiedermann, 'Numerical investigation of turbulent swirling flames with validation in a gas turbine model combustor', *Appl. Therm. Eng.*, vol. 110, pp. 202–212, 2017.

22. Turbulence, heat and mass transfer: *Proceedings of the Seventh International Symposium on Turbulence, Heat and Mass Transfer,ed.by K. Hanjalic, Palermo, Italy, 24-27 September, 2012*.

23. I. V. Novosselov and P. C. Malte, 'Development and application of an eight-step global mechanism for CFD and CRN simulations of lean-premixed combustors', *J. Eng. Gas Turbines Power*, vol. 130, no. 2, 2008.

24. I. Matveev, S. Matveeva, S. Serbin, 'Design and Preliminary Test Results of the Plasma Assisted Tornado Combustor', *Collection of Technical Papers - 43rd AIAA/ASME/SAE/ ASEE Joint Propulsion Conference, Cincinnati, OH*, AIAA 2007-5628, vol. 6, 2007, pp. 6091-6098.

25. G. M. Faeth, 'Structure and atomization properties of dense turbulent sprays', *Symp. (Int.) Combust.*, vol. 23, no. 1, pp. 1345–1352, 1991.

26. S. James, M. Anand, and S. Pope, 'The Lagrangian PDF transport method for simulations of gas turbine combustor flows', in *38th AIAA/ASME/SAE/ASEE Joint Propulsion Conference & Exhibit*, *Indiannapolis, Indiana, USA*, 2002.

27. G. Faeth, 'Spray combustion models - A review', in *17th Aerospace Sciences Meeting, New Orleans, USA,* 1979.

28. W. A. Fiveland and A. S. Jamaluddin, 'Three-dimensional spectral radiative heat transfer solutions by the discrete-ordinates method', *J. Thermophys. Heat Transf.*, vol. 5, no. 3, pp. 335–339, 1991.

29. S. I. Serbin, A. V. Kozlovskyi, and K. S. Burunsuz, 'Investigations of nonstationary processes in low emissive gas turbine combustor with plasma assistance', *IEEE Trans. Plasma Sci. IEEE Nucl. Plasma Sci. Soc.*, vol. 44, no. 12, pp. 2960–2964, 2016.

30. I. B. Matveev, S. I. Serbin, V. V. Vilkul, and N. A. Goncharova, 'Synthesis gas afterburner based on an injector type plasma-assisted combustion system', *IEEE Trans. Plasma Sci. IEEE Nucl. Plasma Sci. Soc.*, vol. 43, no. 12, pp. 3974–3978, 2015.

31. I. Matveev, S. Serbin, T. Butcher, N. Tutu, "Flow Structure investigation in a "Tornado" Combustor," *Collection of Technical Papers - 4th International Energy Conversion Engineering Conference*, vol. 2, 2006, pp. 1001-1013.

32. S. Serbin., A. Kozlovskyi, K. Burunsuz, 'Influence of plasma-chemical products on process stability in a low-emission gas turbine combustion chamber', *International Journal of Turbo and Jet Engines*, 2021. Available from: https://doi.org/10.1515/tjeng-2020-0046.

33. G. F. Romanovsky, S. I. Serbin, V. M. Patlaychuk, *Modern Gas Turbine Units of Russia and Ukraine*. Mikolayiv: NUK, 2005.

34. S. I. Serbin, I. B. Matveev, and G. B. Mostipanenko, 'Plasma-assisted reforming of natural gas for GTL: Part II—modeling of the methane–oxygen reformer', *IEEE Trans. Plasma Sci. IEEE Nucl. Plasma Sci. Soc.*, vol. 43, no. 12, pp. 3964–3968, 2015.

35. S. I. Serbin, I. B. Matveev, and N. A. Goncharova, 'Plasma-assisted reforming of natural gas for GTL—part I', *IEEE Trans. Plasma Sci. IEEE Nucl. Plasma Sci. Soc.*, vol. 42, no. 12, pp. 3896–3900, 2014.

36. I. B. Matveev, A. A. Tropina, S. I. Serbin, and V. Y. Kostyuk, 'Arc Modeling in a Plasmatron Channel', *IEEE Trans. Plasma Sci. IEEE Nucl. Plasma Sci. Soc.*, vol. 36, no. 1, pp. 293–298, 2008.

37. I. Matveev, S. Serbin, A. Mostipanenko, 'Numerical Optimization of the "Tornado" Combustor Aerodynamic Parameters', in *45th AIAA Aerospace Sciences Meeting and Exhibit, Reno, Nevada*, AIAA 2007-391, 2007.

CONTACT WITH THE AUTHORS

Serhiy Serbin
e-mail: serbin1958@gmail.com

Admiral Makarov National University of Shipbuilding,
Geroes of Ukraine, 54025 Mikolayiv,
Ukraine

Badri Diasamidze
e-mail: badri.diasamidze@nuos.edu.ua

Admiral Makarov National University of Shipbuilding,
Geroes of Ukraine, 54025 Mikolayiv,
Ukraine

Viktor Gorbov
e-mail: viktor.gorbov@nuos.edu.ua

Admiral Makarov National University of Shipbuilding,
Geroes of Ukraine, 54025 Mikolayiv,
Ukraine

Jerzy Kowalski
e-mail: jerzy.kowalski@pg.edu.pl

Gdańsk University of Technology,
11/12 Gabriela Narutowicza Street, 80-233 Gdańsk,
Poland